JACS
JOURNAL OF THE AMERICAN CHEMICAL SOCIETY
pubs.acs.org/JACS
Communication

Low-Temperature, Solution-Based Synthesis of Luminescent Chalcogenide Perovskite $BaZrS_3$ Nanoparticles

Ruiquan Yang, Alexander D. Jess, Calvin Fai, and Charles J. Hages*

Cite This: J. Am. Chem. Soc. 2022, 144, 15928−15931
Read Online

ABSTRACT: Chalcogenide perovskites constitute a promising earth-abundant, non-toxic, and robust semiconductor family with the potential to compete with hybrid perovskites as high-quality photovoltaic absorbers. However, a low-temperature, solution-based synthesis route has eluded researchers in this area. Here we report the colloidal synthesis of chalcogenide perovskite $BaZrS_3$ nanoparticles at 330 °C in organic solvent. The nanoparticles (10−20 nm) are found to be comprised of smaller (3−5 nm) crystalline domains. Promising optoelectronic properties for the nanoparticles are measured, with photoluminescence decay times as high as 4.7 ns.

Chalcogenide perovskites—eponymously named for containing S, Se, or Te as the anion rather than a halide—are an emerging frontier in Pb-free, inorganic perovskites with high stability. Promising optoelectronic properties have been identified for this material family, primarily from theory, including band gap values relevant for photovoltaics, a tolerance to deep defects, strong dielectric screening for generating free carriers with a long lifetime, favorable phonon properties for high-performance thermoelectrics, and desirable (isotropic) electron mobility for efficient charge transport.[1−8] Furthermore, a high density of chalcogenide *p*-states in the valence band maximum results in an extraordinarily high absorption coefficient, exceeding those of other solar technologies.[9,10] Importantly, increased covalent bonding in the crystal lattice relative to that in halide perovskites results in enhanced structural stability.[6,11−14]

However, the cost of structural stability for chalcogenide perovskites can be associated with a high crystallization energy barrier for these materials. While chalcogenide perovskites have been sparsely reported for ca. 60 years, the majority of reported syntheses require temperatures around 1000 °C and reaction times on the order of days to weeks (generally using solid-state reaction techniques).[1,5] Such conditions limit the possibility of using most tunable synthesis techniques to control material growth and preclude the majority of substrates commonly used for electronics. The majority of chalcogenide perovskite syntheses also report powders and pellets, which are unrealistic for realizing the properties of chalcogenide perovskites in functional applications. The present high temperature requirements, long synthesis times, and lack of thin-film syntheses are significant barriers to research in chalcogenide perovskites, and the demonstration of solution-based synthesis has been identified as a key goal in chalcogenide perovskite research.[5,6]

In this work, we present the first bottom-up colloidal synthesis of chalcogenide perovskite nanoparticles, demonstrated here for $BaZrS_3$, which is known to crystallize in the desired distorted perovskite crystal structure, shown in the inset of Figure 1. The nanoparticles were synthesized by a thermal decomposition mechanism via the heat-up synthesis technique.[15] First, reactive single-source precursors were synthesized for Ba and Zr (described in the Supporting Information (SI)) as barium dibutyldithiocarbamate (BaDBuDTC) and zirconium diethyldithiocarbamate (ZrDEtDTC),

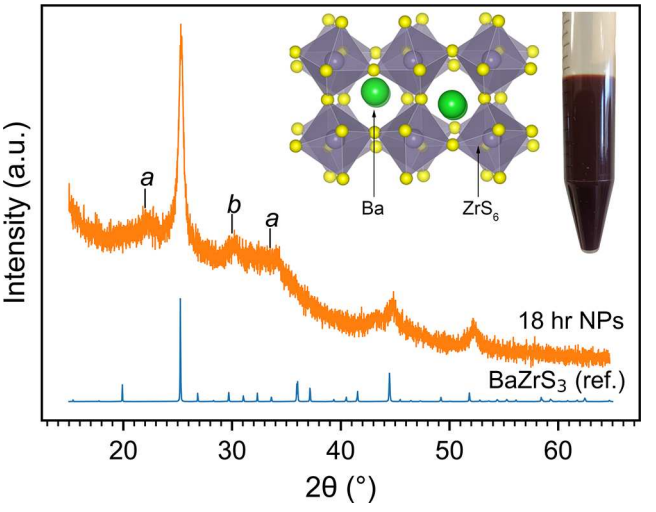

Figure 1. XRD pattern of the $BaZrS_3$ nanoparticles following an 18 h reaction. The reference pattern from Clearfield[16] is shown for comparison. Impurity peaks are labeled with *a* and *b*. The insets show the synthesized nanoparticles as a stable dispersion in toluene and the crystal structure of distorted perovskite $BaZrS_3$.

Received: June 11, 2022
Published: August 24, 2022

https://doi.org/10.1021/jacs.2c06168
J. Am. Chem. Soc. 2022, 144, 15928−15931

respectively. The precursors (0.244 mmol, respectively) were loaded into a homemade reactor with 1 mL of dry oleylamine (OLA) as the solvent/ligand. The mixture was heated (ca. 5 °C/min) to the reaction temperature of 330 °C. BaDBuDTC is fully soluble at ca. 80 °C, while ZrDEtDTC is fully soluble at ca. 120 °C, at which point a clear solution (yellow tint) is formed. Shortly after complete dissolution, the mixture changed to a turbid pale yellow, then orange, and finally dark red over the course of heating, with gaseous byproduct generated during the reaction. Due to the extreme oxophilicity of Zr, the precursors were handled in a glovebox, OLA was dried and degassed prior to use, and the synthesis utilized air-free techniques (Schlenk line) under ultra-high-purity Ar. A series of identical reactions were carried out for various reaction times (0.5, 1, 3, and 18 h). Following the reaction, the product was first dispersed in toluene and isolated by centrifugation (5000 rpm, 5 min). An initial precipitate phase (described below) which does not form a stable dispersion in organic solvent was first separated. The remaining supernatant, containing the target $BaZrS_3$ nanoparticles, was diluted with ethanol as an anti-solvent and recovered via a second centrifugation (10 000 rpm, 5 min). These particles can be kept as a stable dispersion (nanoparticle ink) over weeks without settling, shown in toluene in the inset of Figure 1.

To achieve a low-temperature synthesis, a sufficiently reactive precursor is required. Here metal-dithiocarbamate (DTC)-based precursors were used due to their favorable solubility in organic solvent and low-temperature thermal decomposition (below 300 °C); the decomposition temperature is also tunable based on the choice of organic functional groups (dibutyl and diethyl used here for Ba and Zr, respectively). Individually, these precursors can be used for the synthesis of BaS and ZrS_2. An additional sulfur source is not required for the reactions, as metal-sulfide monomers are directly generated from the thermal decomposition of the metal-DTC. We previously reported the use of metal-DTC precursors for the synthesis of $BaSnS_3$ (non-perovskite needle-like phase) as well as SnS, SnS_2, and ZrS_2,[17−19] and they have also recently been reported for the synthesis of $BaTiS_3$ (non-perovskite hexagonal phase).[20] In general, metal-DTCs are prevalent in the synthesis of metal sulfides and have been reported for the majority of metal cations due to their favorable reactivity, single-source nature for metals and sulfur, and relative ease of synthesis. Importantly, the metal-DTC precursors are free of oxygen (e.g., compared to acetylacetonates and ethers), to prevent oxidation at the reaction temperature. Additionally, common chloride precursors ($ZrCl_4$ and $BaCl_2$) are incompatible with this reaction due to the insolubility of $BaCl_2$ in organic solvents.

Powder X-ray diffraction (XRD) data of the nanoparticles from the longest reaction time (18 h) are shown in Figure 1. The main peaks that can be resolved at 25.2, 44.5, and 52.8° 2θ are in good agreement with the reference for $BaZrS_3$ in the orthorhombic (*Pnma*) distorted perovskite structure.[16] The XRD patterns show clear texturing of the sample, dominated by the (121) or (002) reflections which overlap at 25.2° 2θ; accordingly, parallel reflections from (242) or (004) at 52.8° 2θ also appear with a relatively increased intensity. Such texturing can be expected from anisotropic nanoparticles which can orient in non-random directions during sample preparation.[21] In addition, small impurity peaks labeled *a* and *b* are found. The two peaks labeled *a* were also reported by Comparotto et al.[8] and may be associated with a Zr-rich region, though the origin could not be identified. The peak labeled *b* is a good match for ZrO_2 or $BaZrO_3$; ZrO_2 may form from trace oxygen during synthesis, while $BaZrO_3$ would be a result of minor post-synthesis oxidation of the nanoparticles. XRD patterns for the shorter reaction times (0.5, 1, and 3 h) are virtually identical (see SI). The phase of the $BaZrS_3$ nanoparticles was also verified by Raman spectroscopy (see SI).

A bright-field transmission electron microscopy (TEM) image of nanoparticles from the 18 h reaction is shown in Figure 2a, illustrating a heterogeneous particle size around 10−20 nm. High-resolution TEM (HRTEM) of individual particles indicates that multiple smaller crystalline domains (3−5 nm) exist within a larger particle, illustrated in Figure 2c; lattice fringes with a measured *d*-spacing of 2.88 Å corresponding to the {220} planes are shown. Interestingly, the randomly oriented small domains in Figure 2c predominately show the same fringes of the {220} planes, suggesting preferential growth inside individual nanoparticles. Figure 2b shows another HRTEM image showing different fringes with a measured *d*-spacing of 3.51 and 3.53 Å, corresponding to the

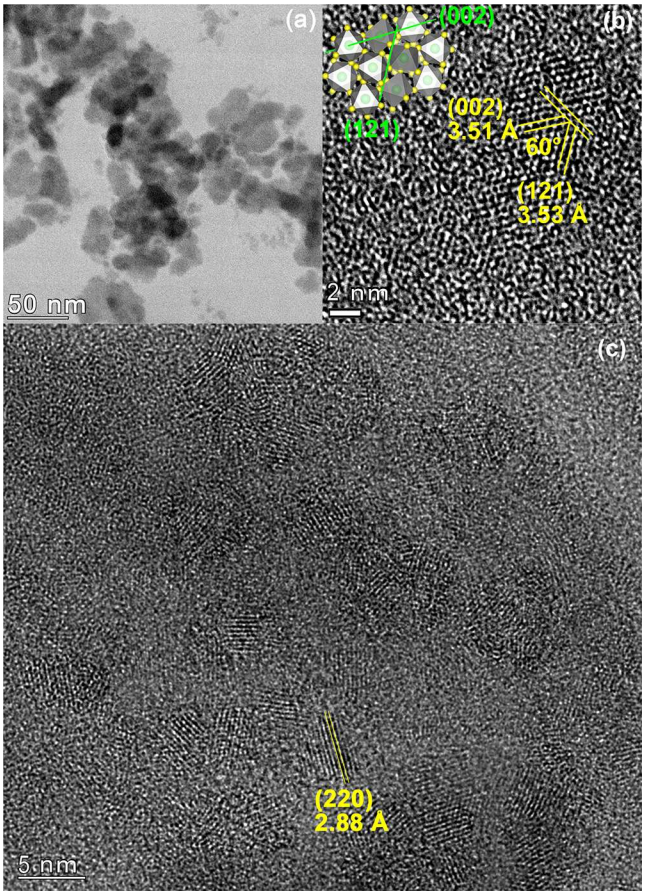

Figure 2. (a) Bright-field TEM image of the $BaZrS_3$ nanoparticles following an 18 h reaction. (b) HRTEM image of a $BaZrS_3$ crystal domain showing (002) and (121) plane fringes; the *d*-spacings and dihedral angle are labeled. The inset shows respective planes in a crystal cell marked with green lines in the same orientation of the crystal domain. (c) HRTEM image of an individual nanoparticle showing multiple crystal domains; (220) plane fringes are shown with the corresponding *d*-spacing labeled.

https://doi.org/10.1021/jacs.2c06168
J. Am. Chem. Soc. 2022, 144, 15928−15931

{002} and {121} planes, respectively; the expected dihedral angle of 60.0° is indicated. The inset of Figure 2b illustrates the structure of $BaZrS_3$ with the (002) and (121) planes indicated. Additional TEM images can be found in the SI as well as for a shorter reaction time (3 h), though a similar morphology and particle size are found, in agreement with the similar XRD.

Optoelectronic properties of the synthesized $BaZrS_3$ were measured with UV−vis and photoluminescence (PL, 532 nm excitation) for the nanoparticles dispersed in toluene. Absorbance data A as a Tauc plot (A^2 vs E, for crystalline semiconductors)[22] is shown for the four reaction times in Figure 3a in comparison to the steady-state PL spectra; PL and

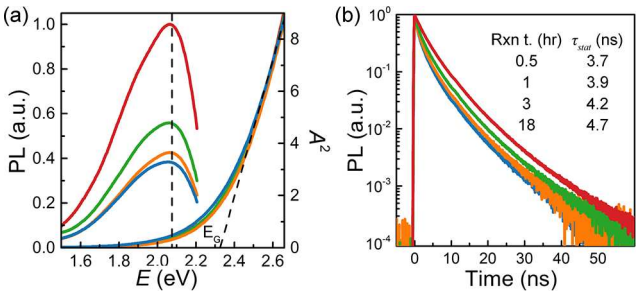

Figure 3. (a) Absorbance (as a Tauc plot) and steady-state PL spectra for various reaction times; the dashed lines indicate the PL peak position and linear fits extrapolated to the band gap (intercept) for the Tauc plot. (b) Normalized TRPL from different reaction times: blue, 0.5 h; orange, 1 h; green, 3 h; red, 18 h.

absorbance data are normalized by their relative sample concentration for comparison. Data for all reaction times yield virtually identical absorbance and emission spectra, with a band gap of ca. 2.3 eV (see SI for details) and a PL peak position at 2.08 eV. A shoulder can be observed in the PL spectra near 1.9 eV. Both the band gap and PL peak position are larger than those reported for bulk $BaZrS_3$ in the literature,[1] which may be attributed to quantum confinement effects originating from the small crystalline domains. Samples with equivalent absorbance show an increase in the steady-state PL yield with increasing reaction time. In agreement, time-resolved PL (TRPL, 532 nm excitation at 9.74 MHz) similarly shows an increase in the PL decay time with increasing reaction time, shown in Figure 3b. As the TRPL is sampled over numerous $BaZrS_3$ particles or domains, we report a statistical lifetime τ_{stat} from a biexponential fit to the PL decay[23] (see SI), which yields 3.7 ± 0.2, 3.9 ± 0.3, 4.2 ± 0.2, and 4.7 ± 0.1 ns for the increasing reactions times, respectively. For comparison, TRPL decay lifetimes have not been previously reported for $BaZrS_3$, though a <7 ns lifetime has been approximated from the steady-state PL yield of a thin film.[1,24] While TRPL in Figure 3b is an integral over the emission spectrum, time-resolved emission spectra shows that the PL spectra decays uniformly in time (see SI).

Based on the preceding results, we speculate the increased reaction time aids in annealing defects in the $BaZrS_3$ nanoparticles. This is not unexpected, as much higher temperatures are typically required for the formation of this phase. We believe the relatively low reaction temperature is also associated with the observed small intraparticle domains, which may uniquely contribute to the observed optoelectronic behavior. Initially, the 0.5 h reaction contains an estimated 50/50 mass ratio of the initial precipitate phase to the target $BaZrS_3$ nanoparticles described herein; this decreases to approximately 20/80 for the 18 h reaction. This initial precipitate phase has similar XRD, TEM, and appearance to the target nanoparticles; however, the instability of the initial precipitates as a dispersion suggests their precipitation is a result of surface properties rather than particle size. Also, a relatively smaller band gap and no PL emission can be detected for this initial precipitate phase (see SI). We speculate this initial precipitate is an intermediate or highly defective $BaZrS_3$ phase which transitions to the target nanoparticles with increasing reaction time.

In summary, we have reported a low-temperature (330 °C), solution-based synthesis for chalcogenide perovskite $BaZrS_3$ nanoparticles. The nanoparticles demonstrate promising optoelectronic properties based on their PL/TRPL, which is encouraging for photovoltaic applications. This result opens the door to using nanoparticle inks[25−27] of chalcogenide perovskite for the realistic fabrication of thin films and devices.

■ ASSOCIATED CONTENT

Supporting Information

The Supporting Information is available free of charge at https://pubs.acs.org/doi/10.1021/jacs.2c06168.

Experimental and measurement details along with supporting materials and optoelectronic characterization data (PDF)

■ AUTHOR INFORMATION

Corresponding Author

Charles J. Hages − *Department of Chemical Engineering, University of Florida, Gainesville, Florida 32611, United States*; orcid.org/0000-0003-4054-1218; Email: c.hages@ufl.edu

Authors

Ruiquan Yang − *Department of Chemical Engineering, University of Florida, Gainesville, Florida 32611, United States*

Alexander D. Jess − *Department of Chemical Engineering, University of Florida, Gainesville, Florida 32611, United States*

Calvin Fai − *Department of Chemical Engineering, University of Florida, Gainesville, Florida 32611, United States*; orcid.org/0000-0001-8866-3674

Complete contact information is available at: https://pubs.acs.org/10.1021/jacs.2c06168

Notes

The authors declare no competing financial interest.

■ ACKNOWLEDGMENTS

C.J.H. acknowledges financial support from the SSMC program at the National Science Foundation (DMR-2044859).

■ REFERENCES

(1) Sopiha, K. V.; Comparotto, C.; Márquez, J. A.; Scragg, J. J. S. Chalcogenide Perovskites: Tantalizing Prospects, Challenging Materials. *Advanced Optical Materials* **2022**, *10*, 2101704.

(2) Jaramillo, R.; Ravichandran, J. In praise and in search of highly-polarizable semiconductors: Technological promise and discovery strategies. *APL Materials* **2019**, *7*, 100902.

(3) Márquez, J. A.; Rusu, M.; Hempel, H.; Ahmet, I. Y.; Kölbach, M.; Simsek, I.; Choubrac, L.; Gurieva, G.; Gunder, R.; Schorr, S.; Unold, T. $BaZrS_3$ Chalcogenide Perovskite Thin Films by H_2S

Sulfurization of Oxide Precursors. *J. Phys. Chem. Lett.* **2021**, *12*, 2148−2153.
(4) Sun, Y.-Y.; Agiorgousis, M. L.; Zhang, P.; Zhang, S. Chalcogenide Perovskites for Photovoltaics. *Nano Lett.* **2015**, *15*, 581−585.
(5) Buffiere, M.; Dhawale, D. S.; El-Mellouhi, F. Chalcogenide Materials and Derivatives for Photovoltaic Applications. *Energy Technology* **2019**, *7*, 1900819.
(6) Swarnkar, A.; Mir, W. J.; Chakraborty, R.; Jagadeeswararao, M.; Sheikh, T.; Nag, A. Are Chalcogenide Perovskites an Emerging Class of Semiconductors for Optoelectronic Properties and Solar Cell? *Chem. Mater.* **2019**, *31*, 565−575.
(7) Comparotto, C.; Ström, P.; Donzel-Gargand, O.; Kubart, T.; Scragg, J. J. Synthesis of $BaZrS_3$ Perovskite Thin Films at a Moderate Temperature on Conductive Substrates. *ACS Applied Energy Materials* **2022**, *5*, 6335−6343.
(8) Comparotto, C.; Davydova, A.; Ericson, T.; Riekehr, L.; Moro, M. V.; Kubart, T.; Scragg, J. Chalcogenide Perovskite $BaZrS_3$: Thin Film Growth by Sputtering and Rapid Thermal Processing. *ACS Applied Energy Materials* **2020**, *3*, 2762−2770.
(9) Nishigaki, Y.; Nagai, T.; Nishiwaki, M.; Aizawa, T.; Kozawa, M.; Hanzawa, K.; Kato, Y.; Sai, H.; Hiramatsu, H.; Hosono, H.; Fujiwara, H. Extraordinary Strong Band-Edge Absorption in Distorted Chalcogenide Perovskites. *Solar RRL* **2020**, *4*, 1900555.
(10) Meng, W.; Saparov, B.; Hong, F.; Wang, J.; Mitzi, D. B.; Yan, Y. Alloying and Defect Control within Chalcogenide Perovskites for Optimized Photovoltaic Application. *Chem. Mater.* **2016**, *28*, 821−829.
(11) Li, W.; Niu, S.; Zhao, B.; Haiges, R.; Zhang, Z.; Ravichandran, J.; Janotti, A. Band gap evolution in Ruddlesden-Popper phases. *Physical Review Materials* **2019**, *3*, 101601.
(12) Ye, K.; Koocher, N. Z.; Filippone, S.; Niu, S.; Zhao, B.; Yeung, M.; Bone, S.; Robinson, A. J.; Vora, P.; Schleife, A.; Ju, L.; Boubnov, A.; Rondinelli, J. M.; Ravichandran, J.; Jaramillo, R. Low-energy electronic structure of perovskite and Ruddlesden-Popper semiconductors in the Ba-Zr-S system probed by bond-selective polarized x-ray absorption spectroscopy, infrared reflectivity, and Raman scattering. *Phys. Rev. B* **2022**, *105*, 195203.
(13) Jess, A.; Yang, R.; Hages, C. J. On the Phase Stability of Chalcogenide Perovskites. *Chem. Mater.* **2022**, *34*, 6894−6901.
(14) Cen, Y.-l.; Shi, J.-j.; Zhang, M.; Wu, M.; Du, J.; Guo, W.-h.; Liu, S.-m.; Han, S.-p.; Zhu, Y.-h. Design of Lead-Free and Stable Two-Dimensional Dion−Jacobson-Type Chalcogenide Perovskite $A'La_2B_3S_{10}$ (A′ = Ba/Sr/Ca; B = Hf/Zr) with Optimal Band Gap, Strong Optical Absorption, and High Efficiency for Photovoltaics. *Chem. Mater.* **2020**, *32*, 2450−2460.
(15) van Embden, J.; Chesman, A. S. R.; Jasieniak, J. J. The Heat-Up Synthesis of Colloidal Nanocrystals. *Chem. Mater.* **2015**, *27*, 2246−2285.
(16) Clearfield, A. The synthesis and crystal structures of some alkaline earth titanium and zirconium sulfides. *Acta Crystallogr.* **1963**, *16*, 135−142.
(17) Yang, R.; Jess, A.; Michalik, J.; Baringer, A.; Hages, C. J. Solution-based synthesis of Chalcogenide Perovskites. *Proceedings of the AIChE 2021 Annual Meeting*; American Institute of Chemical Engineers, 2021.
(18) Yang, R.; Hages, C. J. Solution Synthesis of Regular-Shaped SnS/SnS_2 Van der Waals Heterostructures. *Proceedings of the AIChE 2020 Annual Meeting*; American Institute of Chemical Engineers, 2020.
(19) Michalik, J.; Jess, A.; Yang, R.; Hages, C. J. Solution-based Synthesis of Group 4 Chalcogenide Nanoparticles. *Proceedings of the AIChE 2020 Annual Meeting*; American Institute of Chemical Engineers, 2020.
(20) Ingram, N. E.; Jordan, B. J.; Donnadieu, B.; Creutz, S. E. Barium and titanium dithiocarbamates as precursors for colloidal nanocrystals of emerging optoelectronic materials. *Dalton Transactions* **2021**, *50*, 15978−15982.
(21) Holder, C. F.; Schaak, R. E. Tutorial on Powder X-ray Diffraction for Characterizing Nanoscale Materials. *ACS Nano* **2019**, *13*, 7359−7365.
(22) Zanatta, A. R. Revisiting the optical bandgap of semiconductors and the proposal of a unified methodology to its determination. *Sci. Rep.* **2019**, *9*, 11225.
(23) Hages, C. J.; Levcenco, S.; Miskin, C. K.; Alsmeier, J. H.; Abou-Ras, D.; Wilks, R. G.; Bär, M.; Unold, T.; Agrawal, R. Improved performance of Ge-alloyed CZTGeSSe thin-film solar cells through control of elemental losses. *Progress in Photovoltaics: Research and Applications* **2015**, *23*, 376−384.
(24) Wei, X.; et al. Realization of $BaZrS_3$ chalcogenide perovskite thin films for optoelectronics. *Nano Energy* **2020**, *68*, 104317.
(25) Miskin, C. K.; Yang, W.-C.; Hages, C. J.; Carter, N. J.; Joglekar, C. S.; Stach, E. A.; Agrawal, R. 9.0% efficient $Cu_2ZnSn(S,Se)_4$ solar cells from selenized nanoparticle inks. *Progress in Photovoltaics: Research and Applications* **2015**, *23*, 654−659.
(26) McLeod, S. S. M.; Hages, C. C. J.; Carter, N. N. J.; Agrawal, R. Synthesis and characterization of 15% efficient CIGSSe solar cells from nanoparticle inks. *Progress in Photovoltaics: Research and Applications* **2015**, *23*, 1550−1556.
(27) Guo, Q.; Hillhouse, H. W.; Agrawal, R. Synthesis of Cu_2ZnSnS_4 Nanocrystal Ink and Its Use for Solar Cells. *J. Am. Chem. Soc.* **2009**, *131*, 11672−11673.

https://doi.org/10.1021/jacs.2c06168
J. Am. Chem. Soc. 2022, 144, 15928−15931